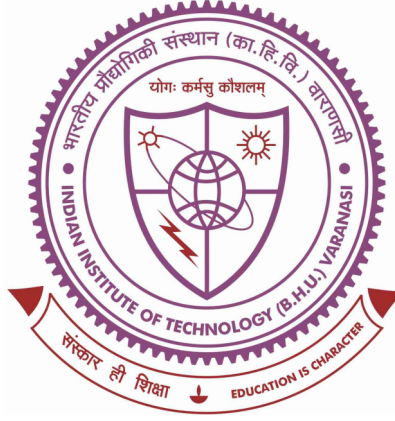


Characterization and Diagnostics of the Localized Flaring Coronae and Their Energetic Responses in Sun-like Stars



Thesis submitted in partial fulfillment for the
Award of Degree

Doctor of Philosophy

By

Shweta Didel

DEPARTMENT OF PHYSICS
INDIAN INSTITUTE OF TECHNOLOGY
(BANARAS HINDU UNIVERSITY)
VARANASI - 221005
INDIA

Roll No. 19171024

Year 2025

CERTIFICATE

It is certified that the work contained in the thesis titled **Characterization and Diagnostics of the Localized Flaring Coronae and Their Energetic Responses in Sun-like Stars** by Ms. **Shweta Didel** (Roll No. **19171024**), in partial fulfillment of the requirement for the award of the degree of Doctor of Philosophy at the **Indian Institute of Technology (B.H.U.), Varanasi** is a record of his own work carried out under my supervision and guidance and this work has not been submitted elsewhere for a degree.

It is further certified that the student has fulfilled all the requirements of the Comprehensive Examination, Candidacy, and SOTA for the award of Ph.D. Degree in Physics.

Abhishek K. Srivastava
27/06/2025
Professor
Department of Physics
Indian Institute of Technology
(Banaras Hindu University)
Varanasi-221005
Supervisor
(Prof. Abhishek K. Srivastava)

Professor
Department of Physics
Indian Institute of Technology
(Banaras Hindu University)
Varanasi-221005

Jeewan C. Pandey

Co-Supervisor

(Dr. Jeewan C. Pandey)

Scientist-F

Aryabhata Research Institute of
Observational Sciences (ARIES)

Manora Peak

Nainital-263001

Declaration

I, **Shweta Didel** (Roll No. **19171024**), certify that the work embodied in this thesis is my own bonafide work and carried out by me under the supervision of **Dr. Abhishekh K. Srivastava** from July 2019 to July 2025 at the *Department of Physics*, Indian Institute of Technology (BHU), Varanasi. The matter embodied in this thesis has not been submitted for the award of any other degree/diploma. I declare that I have faithfully acknowledged and given credits to the research workers whenever and wherever their works have been cited in my work in this thesis. I further declare that I have not wilfully copied any other's work, paragraphs, text, data, results, *etc.*, reported in journals, books, magazines, reports dissertations, thesis, *etc.*, or available at websites and have not included them in this thesis and have not cited as my own work.

Date: June 27, 2025

Place: IIT (BHU), Varanasi

Shweta
27/06/2025
Signature

Shweta Didel

CERTIFICATE BY THE SUPERVISOR

It is certified that the above statement made by the student is correct to the best of my knowledge.

Supervisor

Prof. Abhishekh K. Srivastava

Abhishekh K. Srivastava
27/06/2025
PROFESSOR
Department of Physics
Indian Institute of Technology
(Banaras Hindu University)
Varanasi-221005

J. Pandey

Co-Supervisor

Dr. Jeewan C. Pandey

Signature of the Head of the Department

[Signature]
27/06/25
HEAD/विभागाध्यक्ष
भौतिकी विभाग/Deptt. of Physics
भा0प्रौ0सं0/(का0हि0वि0)/IIT (BHU)
वाराणसी/Varanasi-221005

COPYRIGHT TRANSFER CERTIFICATE

**Title of the Thesis: “Characterization and Diagnostics of the Localized Flaring
Coronae and Their Energetic Responses in Sun-like Stars”**

Name of the Student: Shweta Didel

Copyright Transfer

The undersigned hereby assigns to the Institute of Technology (Banaras Hindu University), Varanasi, all rights under copyright that may exist in and for the above thesis submitted for the award of the “*Doctor of Philosophy*”.

Date: June 27, 2025

Place: IIT (BHU), Varanasi

Shweta
27/06/2025

Signature

Shweta Didel

Note: However, the author may reproduce or authorize others to reproduce material extracted verbatim from the thesis or derivative of the thesis for author’s personal use provided that the source and the Institute’s copyright notice are indicated.

Dedicated to...
My Loving Family

Acknowledgements

First and foremost, I would like to express my heartfelt gratitude to my supervisor, Dr. Abhishekh Kumar Srivastava, for his constant support, guidance, and invaluable insights throughout my PhD journey. His expertise and mentorship have played a crucial role in shaping this work. I am equally thankful to my co-supervisor, Dr. Jeewan C. Pandey, Aryabhata Research Institute of Observational Sciences (ARIES), whose unwavering encouragement, constructive discussions, and thoughtful suggestions have continually motivated and guided me towards becoming a better researcher.

I gratefully acknowledge the Human Resource Development Group (HRDG), Council of Scientific and Industrial Research (CSIR), India, for providing the financial support for this research. I also extend my sincere thanks to the members of the Research Progress Evaluation Committee (RPEC), Dr. Bidya Binay Karak and Dr. Somak Bhattacharyya, for their insightful feedback, thoughtful guidance, and consistent evaluation of my research work throughout the course of my PhD. I am grateful to all the faculty members of the Department and to the non-teaching staff for their timely assistance whenever needed. I sincerely thank my co-authors, Gurpreet Singh and Subhajeet Karmakar, for their collaboration and for their valuable contribution to the research work.

I am deeply grateful to my parents for their unconditional love and support, which has been a constant source of strength and motivation throughout my journey. I also extend my heartfelt thanks to my siblings, Sarita and Vikas, and Jiju for motivating me through this journey. A special mention goes to Misthu and Sunil Bhaskar for bringing joy, love, and warmth into my life, especially during the times I needed it the most.

I am thankful to all my friends and batchmates, especially Neha, Swarnima, Anuvrat, Akanksha, Pratyasha, and Prashant Dixit, for creating unforgettable memories and making this journey more meaningful. I also acknowledge my lab-mates Ritika, Sudheer, Yamini,

Balveer, Kartika, Sripan, and Akash for fostering a positive and collaborative environment and for the constructive discussions. Finally, I would like to express my sincere gratitude to Prof. Patrick Das Gupta for inspiring me to pursue astrophysics. His guidance and humility as a teacher have left a lasting impression on me.

Sincerely

Shweta Didel

List of figures

1.1	The Hertzsprung–Russell (H–R) Diagram for stars in the solar neighbourhood, illustrating the relationship between stellar absolute magnitude, spectral class, temperature, and luminosity. A yellow star symbol marks the location of the Sun, highlighting its position on the main sequence. (Image Credit: Chandra X-ray Observatory, NASA/CXC)	4
1.2	Structure of the Sun: A schematic representation of the Sun’s internal and external layers. The solar interior consists of the core, where nuclear fusion occurs, followed by the radiative zone and the convective zone. The solar atmosphere comprises with the photosphere, chromosphere, and corona. (Image Credit: NASA/Goddard)	6
1.3	The temperature and density variations across different heights or layers of the solar atmosphere. (Image Credit: Kenneth R. Lang (2010))	8
1.4	Schematic representation of the α – Ω dynamo mechanism responsible for generating the solar magnetic field. Starting with a poloidal field (left image), which is transformed into a toroidal field through differential rotation (center image). This leads to the emergence of complex active regions (right image), and the cycle continues as convective motions regenerate the poloidal field. (Image Credit: Carroll and Ostlie (2006)) . . .	9

-
- 1.5 Butterfly diagram illustrating the migration of sunspots over the solar cycle, where sunspots first appear at higher latitudes and gradually shift toward the equator as the cycle progresses. The upper panel shows the distribution of the sunspot area as a function of latitude, where colors indicate the percentage of area coverage, and the lower panel shows the average daily sunspot area variation over time. (Image Credit: Hathaway (2022)) 10
- 1.6 The ratio of X-ray to bolometric luminosity ($R_X = L_X/L_{\text{bol}}$) is plotted against Rossby number ($R_0 = P_{\text{rot}}/\tau_c$). The red dashed line represents the best-fit activity–rotation trends in the saturated regime ($R_0 \leq 0.1$) and the non-saturated regime ($R_0 > 0.1$). (Image Credit: Wright et al. (2011)) . . 14
- 1.7 Left: Full-disk continuum image of active region captured by SOHO/MDI on July 15, 2002. Right: Enlarged view of the sunspot area, highlighting the umbra, penumbra, and surrounding granulation. (Image credit: SOHO [NASA & ESA], Royal Swedish Academy of Sciences) 16
- 1.8 Kepler light curve of solar-type star (KIC 6034120), taken from Notsu et al. (2013), showing periodic brightness variations with respect to average brightness ($\Delta F/F_{\text{av}}$) caused by the rotation of starspots across the stellar disk. The black arrows mark the occurrence of superflares as reported by Maehara et al. (2012) and blue arrows show the position of starspots on the stellar disk through the light-curve modulation. (Image Credit: Notsu et al. (2013)) 17
- 1.9 A solar flare observed on May 5, 2015, by the NASA’s Solar Dynamics Observatory (SDO) is shown in multiple wavelengths of extreme ultraviolet light, each revealing plasma at different temperatures. From left to right, the images display visible light, followed by emissions at 171, 304, 193, and 131 Å. (Image Credit: NASA/GSFC/SDO) 20

-
- 1.10 A change in magnetic topology in a localised diffusion region (shaded) produced by the magnetic reconnection is shown. A plasma element 'A' is initially connected to a plasma element 'B', which gets connected with element 'C' after reconnection. (Image Credit: Pontin and Priest (2022)) . 23
- 1.11 (a) Soft X-ray image of a long-duration solar flare captured by Yohkoh, (b) Schematic illustration of a modified CSHKP flare model adapted from Shibata et al. (1995); Shibata and Magara (2011). 25
- 1.12 (A) The synthetic light curve displaying various segments, including the quiescent, rise, peak, and decay phases of a flare event. (B) An example of a solar flare light curve observed by SphinX spacecraft in the energy range 1.2 - 15 keV is shown. Panel (a) and (b) show the before and after background subtraction light curve with the best-fit flare profile overplotted in red. Panel (c) shows the residual of the best fit. (Image Credit: Gryciuk et al. (2017)) 33
- 1.13 Solar coronal elemental abundances with respect to photospheric values are plotted against First ionization potential (FIP). The data is plotted from previous studies showing low-FIP abundance enhancement and high-FIP depletion with respect to photospheric values, or the so-called FIP effect. (Image Credit: Schmelz et al. (2012)) 36
- 1.14 A graphical representation of FIP bias vs spectral type of the star from G0 to M5. (Image Credit: Wood and Linsky (2010)) 37
- 2.1 Schematic representation of an internal view of the XMM-Newton spacecraft, showing its subsystems and all the main components with outer panels removed for the better visibility. (Image credit: ESA) 42

2.2	(a) Schematic representation of the focusing of X-ray flux through nested Wolter Type-I mirrors, where the paraboloid and hyperboloid surfaces direct incoming X-rays onto the EPIC-PN detector. (b) Illustration of the grating assembly and the division of X-ray flux between the Reflection Grating Spectrometers and the EPIC-MOS detectors. (Image Credit: ESA)	44
2.3	CCD chip assembly in (a) MOS detector and (B) PN detector. (Image Credit: ESA)	45
2.4	Figure showing the PN pattern distribution versus energy (PI channels) as produced by the EPATPLOT task. Panel (a) illustrates the presence of pile-up, evidenced by clear deviations of the single, double, and single+double event distributions from the expected model curves. Panel (b) displays the pattern distribution after pile-up mitigation by excluding the inner core of the source region, resulting in distributions that align closely with the model predictions.	49
2.5	Illustration of the source and background extraction regions on the detector: The solid green circle marks the selected source region centered on the star, while the dashed green circles indicate the nearby background regions used for generating light curves and spectra.	50
3.1	The background subtracted X-ray light curves of AB Dor for different observation epochs. Light curves from PN, MOS, and RGS detectors are shown in blue, black, and red colors, respectively. In order to plot the light curves from all three detectors in the same panel, the MOS count rates are scaled up as $0.8 \times \text{MOS}$ for sets S1 and S2, $5 \times \text{MOS}$ for sets S3, S4, and S6, and $80 \times \text{MOS}$ for set S5. PN count rate is scaled up as $120 \times \text{PN}$ for set S5 and RGS count rate is scaled up as $1.8 \times \text{RGS}$ for set S2.	57

3.2	In the upper panels, PN/RGS light curve (A) and the presence of rotational modulation with best-fit sin curve (B) are shown in violet and black, respectively, for sets S2, S3, S4, and S5. To show the rotational modulation in set S5, the flare part is not shown due to the very high count rate during this flare, F15. The best-fit flare model on the residual (A-B) is shown in the lower panel in black. The regions shaded in light blue color in the upper panel of (a) represent the dimming areas as defined by (Veronig et al., 2021), and the red dotted lines show the level of pre-flare average counts. .	61
3.3	The X-ray spectra of pre- and post-flare states of AB Dor as obtained from the EPIC-PN detector.	65
3.4	Temporal evolution of the spectral parameters of AB Dor during flares and quiescent states, where top to bottom plots show the variation of temperature (T_3) in units of 10^7 K, emission measure (EM_3) in units of 10^{52} cm^{-3} , relative abundance (Z/Z_\odot), and X-ray luminosity in units of $10^{30} \text{ erg s}^{-1}$	67
3.5	Flare evolution in the $\log \sqrt{EM}$ versus $\log(T)$ curve during the decay phase for flares F7, F10, F13, and F20 along with the best fit straight line. The slope (ζ) of the decay path of $\log \sqrt{EM}$ vs. $\log(T)$ is also given in the inset for each flare.	70
4.1	X-ray light curves of HR 1099 in different detectors. The flaring regions are marked by the vertical lines.	86
4.2	Soft and hard X-ray light curves along with the HR curve with 100s binning.	87
4.3	The temporal variation of spectral parameters T_4 , EM_4 , Z , and Luminosity L_{XF} for sets A1 and A2. The T_4 is in units of MK, EM_4 in 10^{53} cm^{-3} , L_{XF} in 10^{31} erg/s . The shaded regions show the peak phase of the corresponding flare.	93

4.4	The density vs temperature (n-T) plot, where $EM^{1/2}$ is considered as the proxy of density. ζ is the slope of the n-T diagram from the decay phase of the flares (a) F1, (b) F2, and (c) F3.	95
4.4	Continued...	96
4.5	Log-log plot of flare duration versus luminosity with linear curve fit.	100
5.1	RGS spectra of AB Dor during quiescent (P11) and flaring state (F20) from the set S6 are shown in green and red color, respectively. The best fit 3-temperature VAPEC model along with the fit for both is shown in blue and black solid lines, respectively.	105
5.2	The RGS1 and RGS2 spectra of pre-flare state P4 and flare F3 for HR 1099 are shown in the upper panel with 3-T VAPEC and 4-T VAPEC models, respectively. The lower panel shows the residuals of the modeled spectra.	107
5.3	Modeled spectra of all the quiescent and flare segments.	108
5.3	Continued...	109
5.3	Continued...	110
5.3	Continued...	111
5.3	Continued...	112
5.4	Elemental abundances plotted as a function of FIP for both quiescent and flaring states during different observations of AB Dor.	113
5.4	Continued...	114
5.4	Continued...	116
5.5	All the elemental abundances relative to Fe are plotted against the first ionization potential (FIP) for HR 1099. The values are provided in Table 5.2.	117
6.1	Temporal evolution of the spectral parameters of AB Dor during flares and quiescent states showing X-ray luminosity in units of 10^{30} erg s^{-1} in top panel and hydrogen column density N_H in units of 10^{20} cm^{-2} in lower panel.	127

6.1 Continued....	128
-------------------	-----

List of tables

1.1	Physical parameters of the Sun (Credit: Priest 2014; Srivastava et al. 2024)	3
1.2	Classification of the flares based on the peak X-ray flux in the wavelength range 1–8 Å (Harra et al., 2016).	22
2.1	Log of the observations of AB Dor and HR 1099 with XMM-Newton.	47
3.1	Basic parameters of AB Dor.	58
3.2	The best-fit model parameters for all the detected flares. Here, F/Q represents the ratio of the flare peak count rate to the quiescent count rate.	60
3.3	Best fit spectral parameters from the pre/post-flare spectra using 3-T APEC model for all data sets.	64
3.4	Loop parameters.	72
3.5	Best fit spectral parameters of each temporal segment of the flares F1-F10, F13, F15, and F20. Here, FS represents flare segments, and ST and ET refer to the start and end times, respectively, of each flare segment relative to the start time of the corresponding observation.	76
4.1	The best-fit parameters for all the observed flares.	89
4.2	Spectral parameters of the quiescent using 4-T APEC model for all the data sets, within a 68% confidence range.	91

4.3	Best fit spectral parameters for each time segment during the flares F1 to F3 within 68% confidence interval.	92
4.4	Loop parameters.	96
5.1	The best-fit optimal spectral parameters derived from fitting the RGS spectra within a 68% confidence level.	115
5.2	Abundances of the elements with respect to Fe in the corona of HR 1099, along with the other observations taken from the literature. All the values are expressed relative to the solar photospheric abundances (Anders and Grevesse, 1989).	120
5.3	Best fit spectral parameters as obtained from the spectral fitting of RGS spectra of AB dor. All the parameters are quoted with a 68 per cent confidence interval.	121
6.1	Best fit spectral parameters of each temporal segment of the flares F1-F10, F13, F15, and F20. Here, FS represents flare segments, and ST and ET refer to the start and end times, respectively of each flare segment relative to the start time of the corresponding observation.	130

Nomenclature of Symbols

R_{\odot}	Radius of the Sun
M_{\odot}	Mass of the Sun
L_{\odot}	Radiation Luminosity of the Sun
g_{\odot}	Solar gravity
K_B	Stefan-Boltzmann constant
κ	Thermal conductivity
n_e	Number density of electrons
p	plasma pressure
β	plasma beta
Z_{\odot}	Solar abundances
N_H	Hydrogen column density
τ_r	Flare rise time
τ_d	Flare decay time
τ_{rad}	Radiative cooling time scale
τ_{cond}	Conduction cooling time scale
M_{CME}	Ejected mass of the CME
R_0	Rossy Number